Biophysical Journal
Article

Biophysical Society

A Beetle Flight Muscle Displays Leg Muscle Microstructure

Toshiki Shimomura,[1] Hiroyuki Iwamoto,[2] Tat Thang Vo Doan,[3] Shin'ichi Ishiwata,[4] Hirotaka Sato,[3,*] and Madoka Suzuki[5,6,7,*]

[1]Department of Physics, Graduate School of Advanced Science and Engineering, Waseda University, Tokyo, Japan; [2]Research and Utilization Division, Japan Synchrotron Radiation Research Institute (JASRI), SPring-8, Hyogo, Japan; [3]School of Mechanical and Aerospace Engineering, Nanyang Technological University, Singapore, Republic of Singapore; [4]Department of Physics, Faculty of Science and Engineering, Waseda University, Tokyo, Japan; [5]WASEDA Bioscience Research Institute in Singapore, Singapore, Republic of Singapore; [6]Comprehensive Research Organization, Waseda University, Tokyo, Japan; and [7]PRESTO, Japan Science and Technology Agency, Saitama, Japan

ABSTRACT In contrast to major flight muscles in the *Mecynorrhina torquata* beetle, the third axillary (3Ax) muscle is a minor flight muscle that uniquely displays a powerful mechanical function despite its considerably small volume, ~1/50 that of a major flight muscle. The 3Ax muscle contracts relatively slowly, and in flight strongly pulls the beating wing to attenuate the stroke amplitude. This attenuation leads to left-right turning in flight or wing folding to cease flying. What enables this small muscle to be so powerful? To explore this question, we examined the microstructure of the 3Ax muscle using synchrotron x-ray diffraction, optical microscopy, and immunoblotting analysis. We found that the 3Ax muscle has long (~5 μm) myofilaments and that the ratio of thick (myosin) filaments to thin (actin) filaments is 1:5 or 1:6. These characteristics are not observed in the major flight muscles, which have shorter myofilaments (~3.5 μm) with a smaller ratio (1:3), and instead are more typical of a leg muscle. Furthermore, the flight-muscle-specific troponin isoform, TnH, is not expressed in the 3Ax muscle. Since such a microstructure is suitable for generating large tension, the 3Ax muscle is appropriately designed to pull the wing strongly despite its small volume.

INTRODUCTION

Insects exhibit amazing modes of locomotion. They float, swim, crawl, jump, run, fly, and even walk on water. They do this with such efficiency, sophistication, and elegance of function across a range of body sizes that they have mastered locomotion on almost every terrain on Earth. This locomotion requires many muscles to enact the required leg and wing movements.

Coleopterans have several well-developed flight muscles, including the dorsal longitudinal muscle (DLM), dorsoventral muscle (DVM), and basalar and subalar muscles (~20 mm in length for the giant flower beetle, *Mecynorrhina torquata*), that are closely packed inside the thorax (Fig. 1). The DLM and DVM are not inserted directly into the wing base but into the cuticles of the thorax, alternately deforming the cuticles and inducing the oscillations that lead the wing to beat at 50–60 Hz. The basalar and subalar muscles are directly inserted into the wing base and alternately pull down the wing base to produce the down and up strokes of the wing (1–5).

Between these major flight muscles, a small muscle, ~50 times smaller than the basalar muscle in volume, is located underneath the wing base and is inserted into the third axillary (3Ax) sclerite, an articulation near the wing base (Fig. 1 *B*). This small flight muscle is thus named the 3Ax muscle. The 3Ax muscle of coleopterans is also known as the wing-folding muscle because, since the 19th century (1,6,7), it was thought to function solely in wing folding. Then, in 2015, Sato et al. (8) discovered that the contraction of the 3Ax muscle pulls the beating wing dorsally to attenuate the wing stroke amplitude to elicit left-right turning in flight. They demonstrated left-right turnings in free flight by electrically stimulating the 3Ax muscles using a miniature radio controller mounted on a flying beetle (8).

The question remains: whichever role the 3Ax muscle performs, be it wing folding or wing stroke attenuation, what feature of this small muscle allows it to be so powerful with such a small volume? To answer this question, in this study we focused our attention on the microstructure of

Submitted April 6, 2016, and accepted for publication August 11, 2016.

*Correspondence: hirosato@ntu.edu.sg or suzu_mado@aoni.waseda.jp

Editor: David Thomas.

http://dx.doi.org/10.1016/j.bpj.2016.08.013

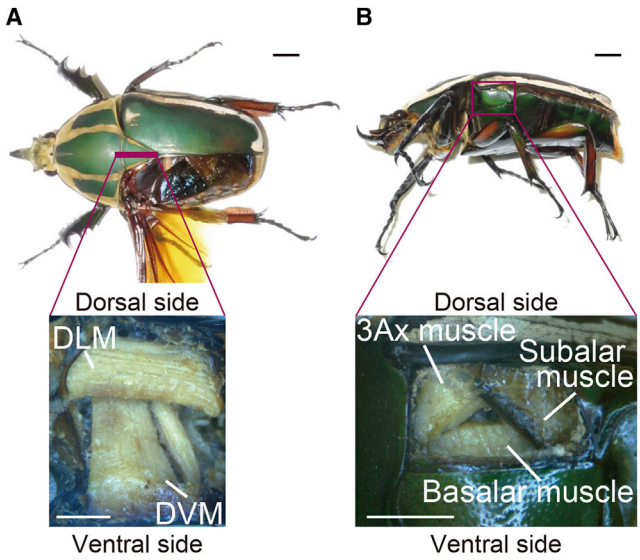

FIGURE 1 Anatomical views of flight muscles in *M. torquata*. (*A* and *B*) Top (*A*) and side (*B*) views of the studied beetle. Bottom: expanded views of the orthogonal section at the thick line (*A*) and of the rectangular area when the cuticle was removed (*B*), highlighting flight muscles tested in this study. Scale bars, 1 cm and 0.5 cm in top and bottom panels, respectively. To see this figure in color, go online.

the muscle. We attempted to quantitatively clarify the microstructure of the 3Ax muscle compared with other flight muscles and a leg muscle by using synchrotron x-ray diffraction (9,10), optical microscopy, and immunoblotting analysis.

Interestingly, the 3Ax muscle has a microstructure that is very distinct from other flight muscles but similar to the leg muscle. This microstructure is appropriately designed for the mechanics required to strongly pull a beating wing using a small muscle volume. We additionally found that the 3Ax muscle does not have a troponin isoform that is specifically and typically expressed in flight muscles, which further indicates that the 3Ax muscle is a uniquely designed motor part compared with other flight muscles.

MATERIALS AND METHODS

Solutions

The relaxing solution consisted of 80 mM KCl, 5 mM $MgCl_2$, 10 mM EGTA, 20 mM imidazole-HCl, pH 7.2, and 4 mM ATP. The glycerol solution comprised 51% glycerol in relaxing solution with 1 mM leupeptin. The relaxing solution for x-ray diffraction measurements contained 80 mM K-propionate, 5 mM $MgCl_2$, 10 mM EGTA, 20 mM imidazole-HCl, pH 7.2, 4 mM ATP, 20 mM creatine phosphate, 125 units/mL creatine phosphokinase, 2 mM dithiothreitol, and 1000 units/mL catalase. The rigor solution for x-ray diffraction measurements contained 80 mM K-propionate, 5 mM EDTA, 5 mM EGTA, 20 mM imidazole-HCl, pH 7.2, 2 mM dithiothreitol, and 1000 units/mL catalase. K-propionate (P0510) was purchased from Tokyo Chemical Industry (Tokyo, Japan). KCl (163-03545), $MgCl_2$ (135-00165), and glycerol (075-00616) were purchased from Wako Pure Chemical Industries (Osaka, Japan). EDTA (345-01865) and EGTA (342-01314) were purchased from Dojindo (Kumamoto, Japan). ATP (A2383), catalase (C40), creatine phosphate (P7936), creatine phosphokinase (C3755), dithiothreitol (D0632), and imidazole (I0125) were purchased from Sigma-Aldrich (St. Louis, MO).

Study animals

M. torquata (order Coleoptera) was used as the model insect (length, 90 ± 9 mm; mass, 6.2 ± 0.8 g; mean ± standard deviation, $n = 5$). Beetles were kept individually in plastic containers (20 cm × 15 cm × 15 cm) with wood chips at the bottom, and fed sugar jelly every 4–5 days at 22.5°C and 37% relative humidity. Studies involving invertebrates, including insects, are exempt from ethics approval by the Science Council of Japan, and Waseda University's regulations for animal experimentation.

Preparation of muscle fibers

Thoraces containing flight muscles with cuticles, and front legs containing leg muscles with cuticles were immersed in a glycerol solution on ice immediately after dissection. The glycerol solution with muscles was turned upside down a few times to mix the solution after 6 h. At 24 h, the glycerol solution was replaced with a new glycerol solution and stored at −20°C for at least 2 weeks.

Optical microscopy

For phase-contrast microscopy, glycerinated muscle fibers were dissected on the day of measurements in relaxing solution. Muscle fibers were placed in a flow cell prepared with two coverslips and double-sided tape. Phase-contrast images were captured under an inverted microscope (IX70, UPlanFL 10XPH, NA 0.30 to observe fibers, and UPlanSApo 100XPH, NA 1.4 to observe myofibrils; both from Olympus, Tokyo, Japan) using an sCMOS camera (Neo; Andor Technology, Antrim, UK) and Andor Solis software (Andor Technology). One camera pixel was 654 nm using a 10× objective, or 64.9 nm using a 100× objective.

For fluorescence microscopy, dissected muscle fibers were immersed in relaxing solution containing either 1 μM (for DLM, DVM, basalar muscle, and subalar muscles), 20 μM (for the 3Ax muscle), or 50 μM (for leg muscles) tetramethylrhodamine-5-maleimide (TMR-maleimide, T-6027; Life Technologies, Waltham, MA) at 4°C for 1.5 h. TMR-maleimide reacts with thiol groups in proteins. In muscle, it stains myosin molecules in the thick filaments and the Z-lines more efficiently than other parts (11). Reacted muscle fibers were centrifuged (1930 *g*, 5 min, 4°C, PMC-060; Tomy Seiko, Tokyo, Japan) and the supernatant was replaced with relaxing solution containing 3% (v/v) formaldehyde. Muscle fibers were resuspended and incubated at 4°C for 1 h. The fixed muscle fibers were then centrifuged again (1930 *g*, 5 min, 4°C) and the supernatant was replaced with relaxing solution containing 0.33 μM Alexa Fluor 488 phalloidin (A12379; Life Technologies). Alexa Fluor 488 phalloidin binds to actin filaments, and thus the Z-line and the thin filaments protruding outward from the Z-line in both directions along the myofibrils (i.e., the I-Z-I brush) become fluorescent. The fluorescence intensity of the Z-line is the highest because the actin filaments overlap at the Z-line. Muscle fibers were resuspended and incubated at 4°C for 15 h. Finally, the stained muscle fibers were placed in a flow cell, washed with relaxing solution, and observed under an inverted microscope (IX71; Olympus) equipped with a 100× oil immersion objective (UPLSAPO 100XO, NA 1.4; Olympus), a spinning disk confocal unit (CSU10; Yokogawa, Tokyo, Japan), and an EM-CCD camera (iXon3 888, DU-888E-C00-#BV; Andor Technology). Alexa Fluor 488 and TMR were respectively excited by 488 nm and 568 nm laser lines from a Krypton Argon ion laser (643-YB-A01; Melles Griot, Rochester, NY) through band-pass filters (FF01-488/6 and FF01-567/15) and a dichroic mirror (Di01-T488/568). Fluorescence cross talk between the green and red channels was confirmed

to be negligible in our imaging conditions (Fig. S1 A in the Supporting Material). The motorized stage, shutters, and camera were controlled by a custom-built LabVIEW program (National Instruments, Austin, TX). One camera pixel was 70.0 nm.

Image analysis

Captured 16-bit images were analyzed using ImageJ software (National Institutes of Health, Bethesda, MD). A rectangle was set as a region of interest (ROI) along the long axis of a myofibril. The average intensity of the short axis of the ROI was plotted at each position of the long axis of the ROI as the intensity profile. The locations of the Z-line and the ends of the A-band, thin filament, and thick filament were determined from the intensity profiles. Data were statistically compared by conducting a one-way analysis of variance with Tukey-Kramer's test.

X-ray diffraction studies

In this study, we used the x-ray diffraction technique, which can clearly and immediately distinguish lattice types without the need for any chemical fixation and staining of the specimen. X-ray diffraction recording was performed at the BL45XU beamline of SPring-8 (12). The x-ray wavelength was 0.1 nm and the specimen-to-detector distance was 2.25 m. The detector was a cooled CCD camera (C4742-98; Hamamatsu Photonics, Hamamatsu, Japan) combined with an image intensifier (VP5445-MOD; Hamamatsu Photonics). The x-ray beams illuminated the glycerinated muscle fibers in an exposure time of 2 s, whereas legs and live beetles were exposed for 200 ms. Given that a single exposure can cause radiation damage to muscles, each region of muscle imaged was exposed only once. A background scattering image was captured without samples and then subtracted from the images with muscles as described previously (13,14). In glycerinated fibers, the illuminated area was shifted along the longitudinal axis of the muscle. We captured 10–20 frames per muscle fiber and averaged the images afterward to improve the signal/noise ratio.

In the recordings with a live beetle, the study animal was tilted by ~45° along the body axis while the legs and wings were fixed using rubber bands and clay. The synchrotron x-ray beam was aimed at one of the wing bases. We first removed the abdominal cuticle to identify the location of the 3Ax muscle (Fig. 1 *B*). The diffraction pattern was then recorded when the x-ray beam was on the 3Ax muscle in the beetle. When the beam was located outside the 3Ax muscle, we obtained the diffraction pattern of neighboring flight muscles, i.e., of basalar or subalar muscles (cf. Figs. 1 *B* and 3). We then set the intact beetle, without removing the cuticles, in the beamline with the same geometry and exposed it to the beam. Although the beetle has thick cuticles, we were able to record the equatorial reflection with a sufficiently high signal/noise ratio. The patterns of the 3Ax muscle acquired from glycerinated fibers and in the fibers dissected fresh from the beetle (within half an hour from dissection until diffraction recording) were essentially the same as those obtained in a live beetle (cf. Fig. S2, C and D), except that the 1,1 and 2,0 reflections were merged in intact and glycerinated specimens, resulting in disordered lattices. This may have been caused by the handling of the specimen, the process of glycerination, and/or endogenous proteases.

To determine the 1,0 lattice spacing, $d1,0$, we first fit the background scattering pattern with the single exponential and subtracted it from those of muscles. We then fit the 1,0 peak with a Gaussian distribution to determine its center of mass. The interfilament distance between the thick filaments was calculated as $2/\sqrt{3} \times d1,0$.

SDS-PAGE and immunoblot analysis

SDS-PAGE and immunoblot analysis were performed as described previously (15). For immunoblotting, the anti-troponin-H antibody from rat (MAC143; ABCAM, Cambridge, UK) and alkaline-phosphatase-conjugated anti-rat IgG from rabbit (A6066; Sigma-Aldrich) were used as the primary and secondary antibodies, respectively. The bands were visualized with BCIP/NBT solution (B6404; Sigma-Aldrich).

RESULTS

Phase-contrast images show clearly striated patterns in the myofibrils from all of the muscles (Fig. 2 *A*). The sarcomere length, which is determined as the distance between adjacent Z-lines, was ~5 μm in the 3Ax muscle, which is significantly larger than that of the other flight muscles (~3.5 μm, $p < 0.001$; Figs. 2, *B* and *C*, and S1 B; Tables S1 and S2) and comparable to that of muscles of the giant waterbug femur (16), tarantula femur (17), and lobster tail (18) (cf. Fig. 4 *A* and Table S4). The longest sarcomere in the beetle was found in leg muscle (~6.3 μm). These trends in the variety of lengths were the same in the A-band width (or the thick-filament length) and the thin-filament length (defined as half of the I-Z-I brush; Figs. 2, *B* and *C*, and S1 B; Tables S1 and S2).

Another difference among the 3Ax and other flight and leg muscles is found in the myofilament lattice structure as examined by synchrotron x-ray diffraction. The diffraction patterns in relaxing conditions recorded from glycerinated fibers of DLM, DVM, basalar, and subalar muscles were typical of flight muscles (Fig. 3), i.e., many layer-line and meridional reflections, in addition to equatorial ones, were clearly recorded due to the near-crystalline order of the contractile proteins (Figs. 3 *A* and S2 A). Their equatorial reflections in relaxing conditions showed the same features as observed in the flight muscles in other species, i.e., the 1,1 reflection was substantially weaker than the 2,0 reflection (19) (Fig. 3; Supporting Discussion). Thus, we conclude that in the myofilament lattice of these muscles, the thick/thin filament ratio is 1:3. From the intensity profiles of equatorial reflections, the 1,0 lattice spacings, $d1,0$, were determined to be between 50.0 and 50.3 nm for DLM, DVM, basalar, and subalar muscles (Fig. 3 *B*; Table S3). The interfilament distance (the distance between the thick filaments; $d1,0 \times 2/\sqrt{3}$) of these flight muscles was calculated to be 57.7–58.1 nm (Table S3).

The diffraction pattern of the 3Ax muscle obtained in live beetles was distinct from those of the other flight muscles (Fig. 3; see Materials and Methods for the details of animal alignment). The 1,1 reflection was as strong as the 2,0 (Fig. 3 *B*). This feature is also different from that observed in vertebrate skeletal muscle: the 1,1 is notably strong, and the weak 2,0 is usually merged with 1,1 as a small peak (Fig. 3; Materials and Methods). This indicates that in the lattice of the 3Ax muscle, the thick/thin filament ratio is neither 1:2 (vertebrate skeletal muscle type) nor 1:3 (flight muscle type). From the intensity profile, we determined a $d1,0$ of 48.5 $\pm$ 1.2 nm ($N = 4$, $n = 7$) and an interfilament distance of 56.0 $\pm$ 1.4 nm (Table S3).

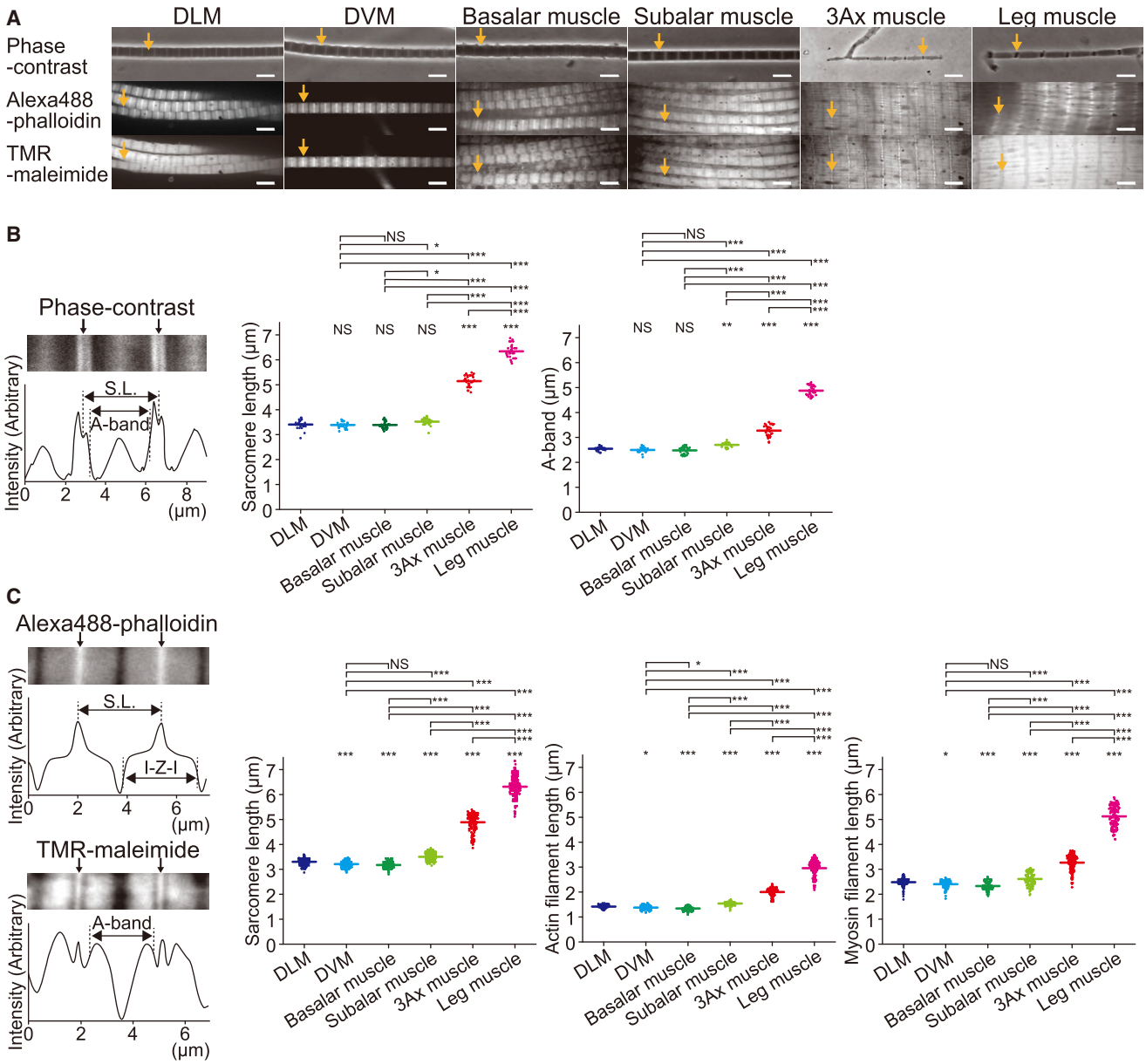

FIGURE 2 Physical dimensions of sarcomeres evaluated by optical microscopy. (*A*) Phase-contrast (*top*) and confocal fluorescence (*middle* and *bottom*) images of myofibrils prepared from glycerinated flight and leg muscles in a relaxing condition. Actin filaments were stained with Alexa Fluor 488 phalloidin after formaldehyde fixation. Myosin filaments were stained with TMR-maleimide. Yellow arrows indicate the Z-lines. (*B*) Sarcomere length and A-band width (myosin filament length) measured in phase-contrast images. Left: a representative image and corresponding intensity profile are shown. The sarcomere length was defined as the distance between the Z-lines indicated by black arrows (marked as S.L. and vertical lines). Another pair of vertical lines (marked as A-band) indicate the midpoints of fluorescence intensity between the highest and lowest intensity values next to the Z-lines. Right: summary of sarcomere lengths and A-bands determined by phase-contrast images. (*C*) Left, top: sarcomere length and I-Z-I brush width (twice that of the thin-filament length) measured from Alexa 488-phalloidin images. The sarcomere length was defined as the distance between the Z-lines indicated by black arrows (marked as S.L. and vertical lines). Another pair of vertical lines (marked as I-Z-I) indicate the midpoints of fluorescence intensity between the points where the intensity begins to decline and the lowest-intensity values. Left, bottom: A-band width measurement in TMR-maleimide images. A pair of vertical lines (marked as A-band) indicate the midpoints of fluorescence intensity between the lowest- and highest-intensity values next to the Z-lines (*black arrows*). Right: summary of sarcomere lengths and lengths of the thin filament (half of the I-Z-I brush width) and thick filament (A-band) obtained from confocal fluorescence images. Means and standard deviations are summarized in Table S1. Scale bars, 5 μm. NS, not significant. $*p < 0.05$, $**p < 0.01$, $***p < 0.001$. Values of the significance tests are summarized in Table S2. To see this figure in color, go online.

The diffraction pattern from intact leg extensor muscle was acquired from a freshly dissected leg with any cuticle left remaining (recorded within half an hour from dissection; Fig. 3 *A*). The 1,1 reflection was stronger than the 2,0, again indicating that the lattice of the leg muscle is different from that of vertebrate skeletal or flight muscles. The d1,0 was

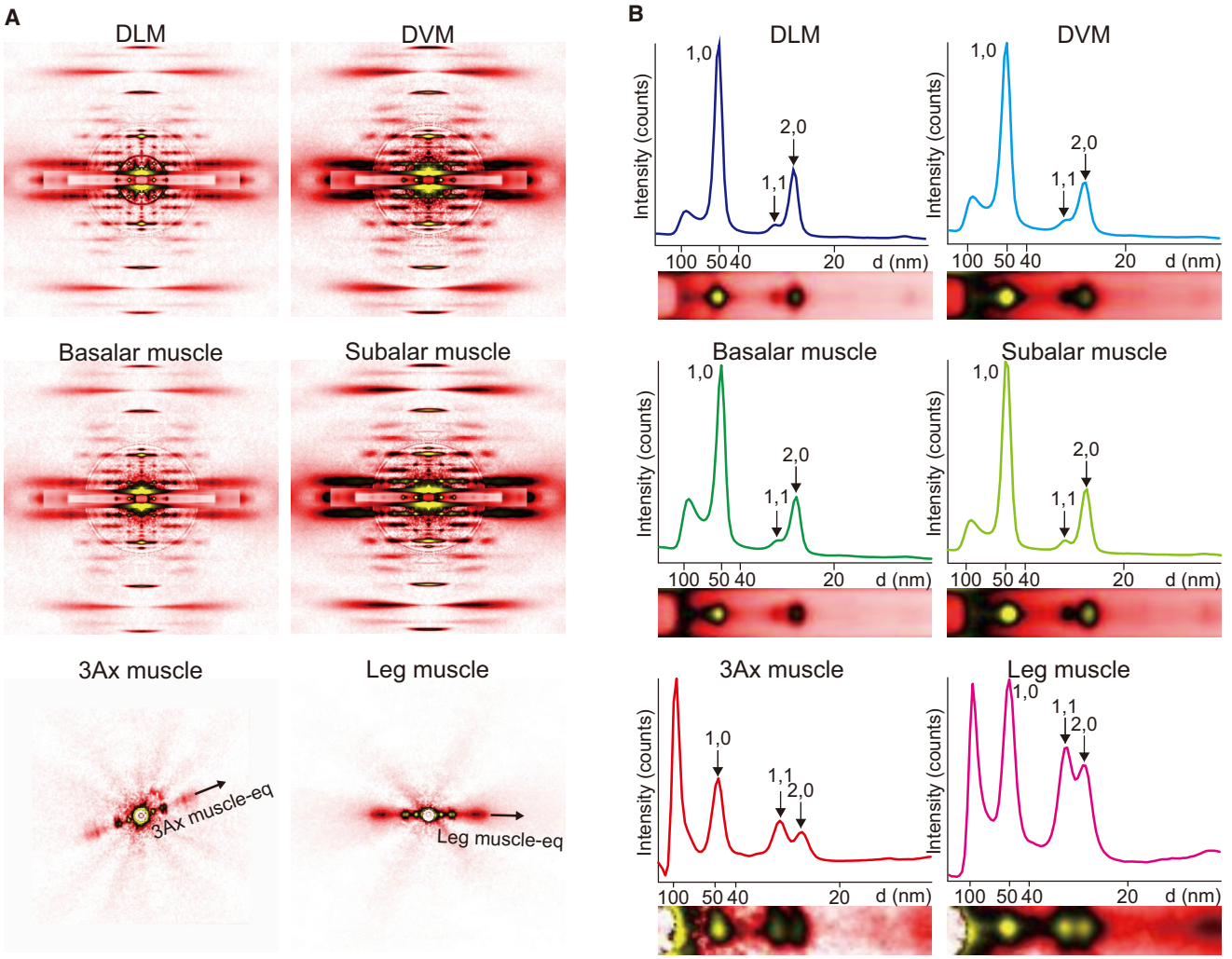

FIGURE 3 Structure of muscles evaluated by synchrotron x-ray diffraction. (*A*) Diffraction patterns recorded from flight and leg muscles. The meridians of the patterns from muscle fibers (the longitudinal axes of the muscle fibers) are oriented vertically. The patterns of the 3Ax muscle and leg muscle were recorded from a live beetle and a freshly dissected leg with its cuticles intact, respectively. (*B*) Magnified views of half of the equatorial reflections and their intensity profiles reproduced from (*A*). To see this figure in color, go online.

determined to be 50.1 ± 1.1 nm ($N = 2$, $n = 2$) and the interfilament distance was 57.8 ± 1.2 nm (Table S3).

The 3Ax muscle also differs from other flight muscles in muscle protein composition. Flight muscles have a long Pro-Ala-rich extension, usually at the C-terminus of troponin-I (20), and in some species, such as *Drosophila*, at the C-terminus of tropomyosin (21,22). Given that the apparent molecular mass of such a flight-muscle-specific troponin-I isoform on a gel (70–80 kDa) is greater than that of non-flight-muscle troponin-I isoforms (~25 kDa), this isoform is often referred to as TnH (where H stands for heavy) (20). As shown in Fig. S4 A, the SDS-PAGE patterns from DLM, DVM, basalar, and subalar muscles are quite similar to one another but are significantly less similar to that obtained from the 3Ax muscle. The band corresponding to the ~75 kDa protein was commonly seen in the major four muscles but was absent from the 3Ax muscle. Immunoblotting shows that an antibody against TnH (MAC143) cross-reacted with the ~75 kDa bands in all four major flight muscles, but not in the 3Ax muscle. The ~75 kDa protein likely corresponds to the TnH of *M. torquata*, suggesting that TnH is not expressed in the 3Ax muscle (Fig. S4 B). Additionally, the dissimilar band pattern in the lower-mass region of the 3Ax muscle suggests different isoform expressions of, e.g., troponin subunits and myosin light chains compared with the other flight muscles.

DISCUSSION

Based on the optical microscopy data, the sarcomere and thick and thin filaments were confirmed to be significantly longer in the 3Ax muscle than in the DLM, DVM, basalar, and subalar muscles, and longest in the leg muscle. X-ray diffraction patterns revealed a thick/thin filament ratio of

1:3 and an ordered protein arrangement in DLM, DVM, basalar, and subalar muscles. In contrast, a greater thick/thin filament ratio was detected in both the 3Ax and leg muscles. The similarities in morphology and TnH expression among the DLM, DVM, basalar, and subalar muscles found here suggest that the well-developed basalar and subalar muscles in *M. torquata* (cf. Fig. 1) are asynchronous muscles, i.e., the tension generation of the muscle is not tightly synchronized with each nerve impulse or the cycle of cytosolic Ca^{2+} increase and decrease (9,23,24). Therefore, these muscles provide the power for wing oscillation just as they do in another coleopteran, *Cotinus mutabilis* (25,26). It should be noted that there are synchronous flight muscles that express TnH (e.g., in *Manduca sexta*, *Periplaneta americana*, and *Schistocerca gregaria*) (27) and/or have packing structures similar to those observed in asynchronous muscles (e.g., the basalar muscle of *Achalarus lyciades*) (28). In the leg muscle, the thick/thin filament ratio was 1:5 or 1:6, as is found in many other slow-acting invertebrate muscles (cf. Fig. 4, *D* and *E*, and Table S4). This ratio can be inferred from the comparable intensities of the 1,1 and 2,0 reflections in x-ray diffraction patterns (19,29) (Fig. S3; Supporting Discussion). A similar pattern was obtained from the 3Ax muscle (Fig. 3), suggesting that the thick/thin filament ratio of this flight muscle is of the leg type, i.e., 1:5 or 1:6. We also confirmed that among the flight muscles tested in the beetle, only the 3Ax muscle does not have TnH, which serves as a scaffold in asynchronous flight muscles to maintain the integrity of the flight-muscle-specific 1:3 lattice (15,19).

The sarcomere and myofilament lengths, as well as the filament number ratio and protein composition, were heterogeneous inside the beetle's small body. This variety likely represents the variation of mechanical functions among the muscles. The fast-acting flight muscle has shorter sarcomeres and its amplitude of oscillation in living insects is ~3% of its length (30). In contrast, the relatively long sarcomeres of the 3Ax muscle are reminiscent of a leg muscle. When only the sarcomere length is considered, and other factors such as the filament number ratio and the gliding speed of actomyosin are the same, the speed of contraction is proportional to the number of sarcomeres in the muscle, whereas a greater number of cross-bridges per sarcomere provides higher tension (31,32). The longer thick and thin filaments (i.e., the longer overlap region between the thick and thin filaments) in the 3Ax and leg muscles suggest that the physiological requirement of these muscles is to produce high tension rather than fast contraction.

To further investigate these structural insights and their physiological implications for muscles in the beetle, we graphically show the correlations among filament length, sarcomere length, thick/thin filament ratio, and interfilament distance in the beetle and other vertebrates and invertebrates studied elsewhere (Fig. 4; Table S4) (16–18,29,33–49). Here, the universal trend is that the sarcomere length correlates positively with both the thick- and thin-filament lengths (Fig. 4, *A* and *B*), and the thin-filament lengths correlate with the thick-filament lengths (Fig. 4 *C*). Furthermore, the linear correlations that exist across the whole animal kingdom are clearly observed even within the beetle (*colored plots* in Figs. 4, *A–C*). Such correlations in a single species were previously observed in the leg muscles of crabs. Franzini-Armstrong (33) demonstrated the variability within single fibers, and reported that the thin-filament length correlated proportionally with the length of half the thick filament. These data indicate that a common mechanism to determine myofilament lengths is built into the sarcomeres of different species. Such a coordinated growth of both myofilaments can effectively increase the overlap length of these filaments, so that the functional requirements of each muscle are fulfilled.

When the thick-filament length is plotted against the thick/thin filament ratio, again the universal trend is linear (Fig. 4 *D*). The leg muscles of the beetle are at the longer end among the muscles with higher filament ratios (>1:5), whereas the 3Ax muscle is at the shorter end among these muscles, i.e., the thick filament is the shortest in the group. With the same overlap length of the thin and thick filaments, a larger filament ratio provides a greater number of myosin cross-bridges, leading to higher tension if a sufficient number of myosin heads are provided and all other conditions are the same (i.e., if the effect of the interfilament distance on tension is not considered, as discussed below). The observed distribution of values in the beetle suggests that the maximum tension required in the 3Ax muscle is higher than that in other flight muscles but less than that in the leg muscle of this beetle.

The interfilament distance has a direct impact on the production of tension. We previously showed that tension is maximized at the optimal spacing in rabbit psoas myofibrils (50). As the thick/thin filament ratio increases, the density of the thin filaments surrounding one thick filament increases, unless the interfilament distance is enlarged. This situation should negatively affect tension generation. It is therefore expected that the interfilament distance is matched with the thick/thin filament ratio to optimize the tension. As expected, the correlation between the interfilament distance and the thick/thin filament ratio is proportional, i.e., the muscle with a higher thick/thin filament ratio has a larger interfilament distance (Fig. 4 *E*). However, despite the variety of thick/thin filament ratios found in the beetle, all of the muscles tested here had similar interfilament distances (Table S3). Skinned muscle fibers of the DLM, DVM, basalar, and subalar muscles were subjected to x-ray diffraction studies, whereas intact muscles were studied in the 3Ax and leg muscles. Given that the spacing is 10–20% greater in skinned muscle fibers than in intact muscles due to swelling (cf. Fig. S2, C and D) (51,52), the spacing of the DLM, DVM, basalar, and subalar muscles in the intact condition is potentially 10–20% narrower than that of the 3Ax and leg muscles. Taking this into

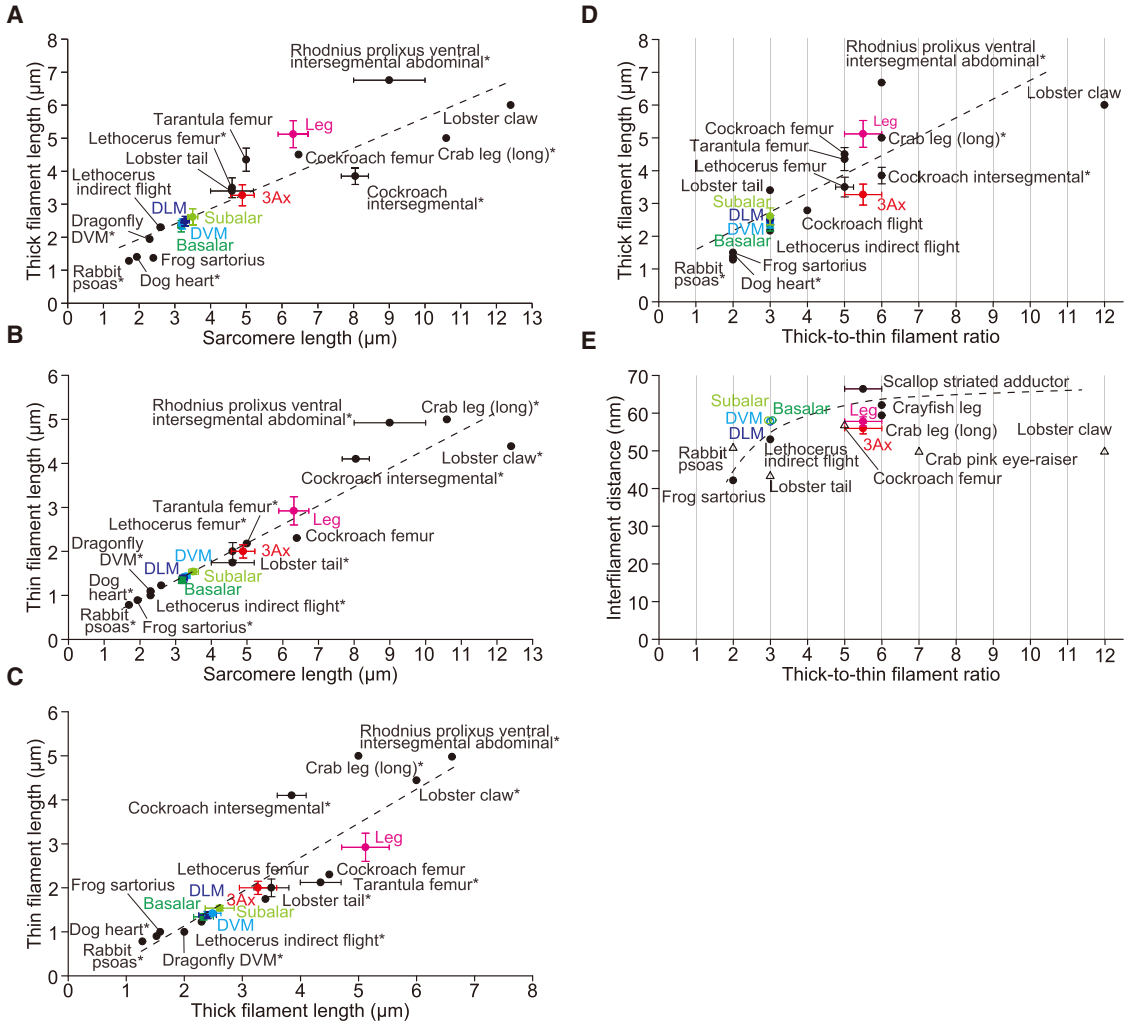

FIGURE 4 Correlations among the filament length, sarcomere length, thick/thin filament ratio, and interfilament distance. (*A–E*) Correlations between the lengths of sarcomeres and the thick filaments (*A*), between the lengths of sarcomeres and thin filaments (*B*), between the lengths of thick and thin filaments (*C*), between the thick/thin filament ratio and the thick-filament length (*D*), and between the thick/thin filament ratio and the interfilament distance of the thick filaments (*E*). The plots include the values determined in this study (*color coded*) and in previous studies (*black*). Solid circles, x-ray diffraction recordings from intact muscles; open circles, x-ray diffraction recordings from glycerinated muscles; open triangles, electron microscopy. For some data (*), we estimated the values based on the images provided in each reference. Error bars show standard deviations determined in this study or the range of parameters described in references. In (*E*), error bars for DVM, DLM, basalar, and subalar muscles are not shown because they overlap with the plots. Broken lines show the linear fit: $y = 0.45x + 1.09$, $R^2 = 0.79$ in (*A*); $y = 0.44x + 0.01$, $R^2 = 0.92$ in (*B*); $y = 0.79x + 0.42$, $R^2 = 0.76$ in (*C*); and $y = 0.52x + 1.08$, $R^2 = 0.66$ in (*D*). In (*E*), a broken-line curve is drawn to guide the eye. See Tables S1, S3, and S4 for exact values.

consideration, the plots obtained from the beetle follow the global trend.

The physical dimensions and the structure of the 3Ax muscle can reasonably be assumed to provide a mechanical function in flight, as its structural parameters lie between those of fast-acting flight and slow-acting leg muscles. Sato et al. (8) recently employed electrical stimulation in a free-flying condition to prove that the 3Ax muscle steers the flight of this beetle. This small muscle is activated in such a way as to cause tonic contraction (i.e., the period of time in which the muscle is activated is much longer than that for a single wing stroke) to alter the amplitude of the wing stroke, leading to turning in flight, while the other four major flight muscles powerfully oscillate the thorax and wings. To perform such a mechanical function with a small volume, the 3Ax muscle likely needs to produce sufficiently strong tension to alter the amplitude of the powerfully flapping wing. At the same time, the muscle needs to contract quickly enough, probably faster than the leg muscles, to steer the beetle in the desired directions.

In summary, by using optical microscopy, in vivo x-ray diffraction recordings, and immunoblotting analyses of *M. torquata* beetle muscles, we found that the beetle has a small flight muscle that is distinct from its other flight muscles but is similar to its leg muscle in ultrastructure. The structural difference among the 3Ax and other flight and

leg muscles is explained by the difference in their physiological roles. The linear structure-function correlation commonly seen across the animal kingdom is present even within the compact structure of this beetle species. These results further highlight the importance of matching a muscle's ultrastructure with its role in each specific body part. Perturbations in the length of the myofilaments and the interfilament distance, as shown in the soleus muscle fibers of the rat under disuse, could cause a substantial decrease in the active force (11). In light of the challenges facing stem-cell therapies for muscle diseases, these insights into the muscular structure-function relationship could perhaps lead to a means to gauge in advance how well engineered muscle cells will integrate structurally and functionally into a target site (53).

SUPPORTING MATERIAL

Supporting Discussion, four figures, and four tables are available at http://www.biophysj.org/biophysj/supplemental/S0006-3495(16)30701-9.

AUTHOR CONTRIBUTIONS

S.I., H.S., and M.S. designed the research. T.S., H.I., and T.T.V.D. performed experiments. T.S. and H.I. analyzed data. T.S., H.I., H.S., and M.S. wrote the manuscript. All authors discussed the results and commented on the manuscript.

ACKNOWLEDGMENTS

We thank Dr. M. Miyazaki for providing the software to control the microscopy system.

This research was partially supported by the MOE Academic Research Fund in Singapore (Tier 1 grant RG41/15 to H.S.), the Japan Society for the Promotion of Science (KAKENHI grant number 22227005 to S.I.), an Agency for Science, Technology and Research (A*STAR) - Japan Science and Technology Agency (JST) joint grant (to S.I. and H.S.), and PRESTO, JST (to M.S.). The synchrotron radiation experiments were performed at SPring-8 in Japan with the approval of the Japan Synchrotron Radiation Research Institute (proposal No. 2015A1502, 2015B1449, 2016A1169).

REFERENCES

1. Snodgrass, B. R. E. 1909. The thorax of insects and the articulations of the wings. *Proc. U.S. Natl. Mus.* 36:511–595.
2. Pringle, J. W. S. 1957. Insect Flight. Cambridge University Press, Cambridge, UK.
3. Darwin, F. W., and J. W. S. Pringle. 1959. The physiology of insect fibrillar muscle. II. Mechanical properties of a beetle flight muscle. *Proc. R. Soc. Lond. B Biol. Sci.* 151:194–203.
4. Sato, H., C. W. Berry, …, M. M. Maharbiz. 2009. Remote radio control of insect flight. *Front. Integr. Nuerosci.* 3:24.
5. Burton, A. J. 1971. Directional change in a flying beetle. *J. Exp. Biol.* 54:575–585.
6. Stellwaag, F. 1914. Der Flugapparat der Lamellicornier. *In* Zeitschrift für Wissenschaftliche Zoologie. K. von Albert, K. T. E. von Seibold, and E. H. Ehlers, editors. Wilhelm Engelmann, Leipzig, Germany.
7. Straus-Durckheim, H. 1828. Considérations Générales sur l'Anatomie Comparée des Animaux Articulés: Auxquelles on a Joint l'Anatomie Descriptive du *Melolontha vulgaris* (Hanneton), Donnée comme Exemple de l'Organisation des Coléoptères, Vol. 1. Levrault, Paris.
8. Sato, H., T. T. Vo Doan, …, M. M. Maharbiz. 2015. Deciphering the role of a coleopteran steering muscle via free flight stimulation. *Curr. Biol.* 25:798–803.
9. Iwamoto, H., and N. Yagi. 2013. The molecular trigger for high-speed wing beats in a bee. *Science.* 341:1243–1246.
10. Dickinson, M., G. Farman, …, T. Irving. 2005. Molecular dynamics of cyclically contracting insect flight muscle in vivo. *Nature.* 433:330–334.
11. Udaka, J., S. Ohmori, …, N. Fukuda. 2008. Disuse-induced preferential loss of the giant protein titin depresses muscle performance via abnormal sarcomeric organization. *J. Gen. Physiol.* 131:33–41.
12. Fujisawa, T., K. Inoue, …, T. Ueki. 2000. Small-angle X-ray scattering station at the SPring-8 RIKEN beamline. *J. Appl. Cryst.* 33:797–800.
13. Iwamoto, H., J. Wakayama, …, N. Yagi. 2003. Static and dynamic x-ray diffraction recordings from living mammalian and amphibian skeletal muscles. *Biophys. J.* 85:2492–2506.
14. Iwamoto, H., K. Inoue, and N. Yagi. 2010. Fast x-ray recordings reveal dynamic action of contractile and regulatory proteins in stretch-activated insect flight muscle. *Biophys. J.* 99:184–192.
15. Iwamoto, H. 2013. The long C-terminal extension of insect flight muscle-specific troponin-I isoform is not required for stretch activation. *Biochem. Biophys. Res. Commun.* 431:47–51.
16. Tregear, R. T., and J. M. Squire. 1973. Myosin content and filament structure in smooth and striated muscle. *J. Mol. Biol.* 77:279–290.
17. Levine, R. J. C., R. W. Kensler, …, H. A. King. 1983. Structure and paramyosin content of tarantula thick filaments. *J. Cell Biol.* 97:186–195.
18. Hayes, D., M. Huang, and C. R. Zobel. 1971. Electron microscope observations on thick filaments in striated muscle from the lobster Homarus americanus. *J. Ultrastruct. Res.* 37:17–30.
19. Iwamoto, H. 2013. Flight muscle-specific Pro-Ala-rich extension of troponin is important for maintaining the insect-type myofilament lattice integrity. *J. Struct. Biol.* 183:33–39.
20. Bullard, B., K. Leonard, …, E. Fyrberg. 1988. Troponin of asynchronous flight muscle. *J. Mol. Biol.* 204:621–637.
21. Karlik, C. C., and E. A. Fyrberg. 1986. Two Drosophila melanogaster tropomyosin genes: structural and functional aspects. *Mol. Cell. Biol.* 6:1965–1973.
22. Hanke, P. D., and R. V. Storti. 1988. The Drosophila melanogaster tropomyosin II gene produces multiple proteins by use of alternative tissue-specific promoters and alternative splicing. *Mol. Cell. Biol.* 8:3591–3602.
23. Ellington, C. P. 1985. Power and efficiency of insect flight muscle. *J. Exp. Biol.* 115:293–304.
24. Dickinson, M. H., and M. S. Tu. 1997. The function of dipteran flight muscle. *Comp. Biochem. Physiol. A Physiol.* 116:223–238.
25. Josephson, R. K., J. G. Malamud, and D. R. Stokes. 2000. Asynchronous muscle: a primer. *J. Exp. Biol.* 203:2713–2722.
26. Josephson, R. K., J. G. Malamud, and D. R. Stokes. 2000. Power output by an asynchronous flight muscle from a beetle. *J. Exp. Biol.* 203:2667–2689.
27. Peckham, M., R. Cripps, …, B. Bullard. 1992. Mechanics and protein-content of insect flight muscles. *J. Exp. Biol.* 168:57–76.
28. Reger, J. F., and D. P. Cooper. 1967. A comparative study on the fine structure of the basalar muscle of the wing and the tibial extensor muscle of the leg of the lepidopteran Achalarus lyciades. *J. Cell Biol.* 33:531–542.
29. Elliott, G. F., J. Lowy, and C. R. Worthington. 1963. An X-ray and light-diffraction study of the filament lattice of striated muscle in the living state and in rigor. *J. Mol. Biol.* 6:295–305.

30. Chan, W. P., and M. H. Dickinson. 1996. In vivo length oscillations of indirect flight muscles in the fruit fly Drosophila virilis. *J. Exp. Biol.* 199:2767–2774.

31. Jahromi, S. S., and H. L. Atwood. 1969. Correlation of structure, speed of contraction, and total tension in fast and slow abdominal muscle fibers of the lobster (Homarus americanus). *J. Exp. Zool.* 171:25–38.

32. Huxley, A. F., and R. Niedergerke. 1954. Structural changes in muscle during contraction; interference microscopy of living muscle fibres. *Nature.* 173:971–973.

33. Franzini-Armstrong, C. 1970. Natural variability in the length of thin and thick filaments in single fibres from a crab, Portunus depurator. *J. Cell Sci.* 6:559–592.

34. Yagi, N., and I. Matsubara. 1977. The equatorial x-ray diffraction patterns of crustacean striated muscles. *J. Mol. Biol.* 117:797–803.

35. Hoyle, G. 1967. Diversity of striated muscle. *Am. Zool.* 7:435–449.

36. April, E. W., P. W. Brandt, and G. F. Elliott. 1971. The myofilament lattice: studies on isolated fibers. I. The constancy of the unit-cell volume with variation in sarcomere length in a lattice in which the thin-to-thick myofilament ratio is 6:1. *J. Cell Biol.* 51:72–82.

37. Brandt, P. W., J. P. Reuben, …, H. Grundfest. 1965. Correlated morphological and physiological studies on isolated single muscle fibers. I. Fine structure of the crayfish muscle fiber. *J. Cell Biol.* 25 (3, Suppl):233–260.

38. Spotnitz, H. M., E. H. Sonnenblick, and D. Spiro. 1966. Relation of ultrastructure to function in the intact heart: sarcomere structure relative to pressure volume curves of intact left ventricles of dog and cat. *Circ. Res.* 18:49–66.

39. Stenger, R. J., and D. Spiro. 1961. The ultrastructure of mammalian cardiac muscle. *J. Biophys. Biochem. Cytol.* 9:325–351.

40. Smith, D. S. 1966. The organization of flight muscle fibers in the Odonata. *J. Cell Biol.* 28:109–126.

41. Millman, B. M., T. J. Racey, and I. Matsubara. 1981. Effects of hyperosmotic solutions on the filament lattice of intact frog skeletal muscle. *Biophys. J.* 33:189–202.

42. Hodge, A. J., H. E. Huxley, and D. Spiro. 1954. Electron microscope studies on ultrathin sections of muscle. *J. Exp. Med.* 99:201–206.

43. Reedy, M. K. 1967. Cross-bridges and periods in insect flight muscle. *Am. Zool.* 7:465–481.

44. Podolsky, R. J. 1972. Contractility of Muscle Cells and Related Processes. Prentice-Hall, Englewood Cliffs, NJ.

45. Toselli, P. A., and F. A. Pepe. 1968. The fine structure of the ventral intersegmental abdominal muscles of the insect Rhodnius prolixus during the molting cycle. II. Muscle changes in preparation for molting. *J. Cell Biol.* 37:462–481.

46. Millman, B. M., P. M. Bennett, and P. M. Bennett. 1976. Structure of the cross-striated adductor muscle of the scallop. *J. Mol. Biol.* 103:439–467.

47. Hagopian, M. 1966. The myofilament arrangement in the femoral muscle of the cockroach, Leucophaea maderae fabricius. *J. Cell Biol.* 28:545–562.

48. Hagopian, M., and D. Spiro. 1967. The sarcoplasmic reticulum and its association with the T system in an insect. *J. Cell Biol.* 32:535–545.

49. Smith, D. S. 1966. The structure of intersegmental muscle fibers in an insect, Periplaneta americana L. *J. Cell Biol.* 29:449–459.

50. Shimamoto, Y., F. Kono, …, S. Ishiwata. 2007. Nonlinear force-length relationship in the ADP-induced contraction of skeletal myofibrils. *Biophys. J.* 93:4330–4341.

51. Magid, A., and M. K. Reedy. 1980. X-ray diffraction observations of chemically skinned frog skeletal muscle processed by an improved method. *Biophys. J.* 30:27–40.

52. Irving, T. C., J. Konhilas, …, P. P. de Tombe. 2000. Myofilament lattice spacing as a function of sarcomere length in isolated rat myocardium. *Am. J. Physiol. Heart Circ. Physiol.* 279:H2568–H2573.

53. Segers, V. F. M., and R. T. Lee. 2008. Stem-cell therapy for cardiac disease. *Nature.* 451:937–942.

Biophysical Journal, Volume *111*

Supplemental Information

A Beetle Flight Muscle Displays Leg Muscle Microstructure

Toshiki Shimomura, Hiroyuki Iwamoto, Tat Thang Vo Doan, Shin'ichi Ishiwata, Hirotaka Sato, and Madoka Suzuki

Supporting Figures

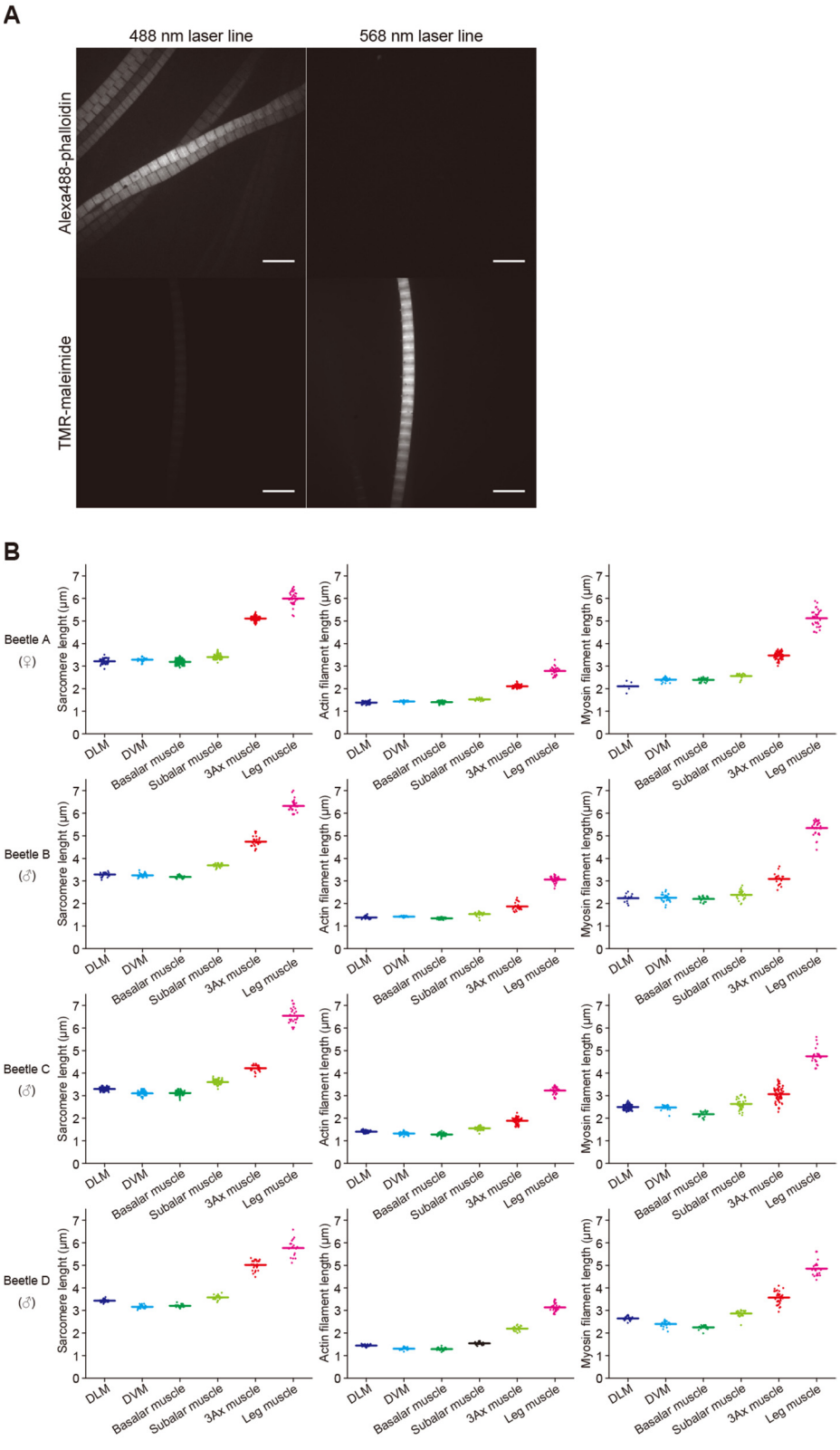

Figure S1 Confocal fluorescence microscopy of flight and leg muscles.

(*A*) Cross-talk between Alexa Fluor 488 and TMR in confocal microscopy setup. Fluorescence images of myofibrils of DLM co-labeled with Alexa488-phalloidin (top) and TMR-maleimide (bottom). Images were acquired with laser excitation of 488 nm (left) or 568 nm (right). Alexa Fluor 488 fluorescence was undetectable with 568 nm excitation (top, right). Although TMR fluorescence was observed with 488 nm excitation, it was negligibly weaker than Alexa Fluor 488 fluorescence. Scale bars, 10 μm. (*B*) Sarcomere, myosin filament and actin filament lengths in each animal determined from confocal fluorescence images.

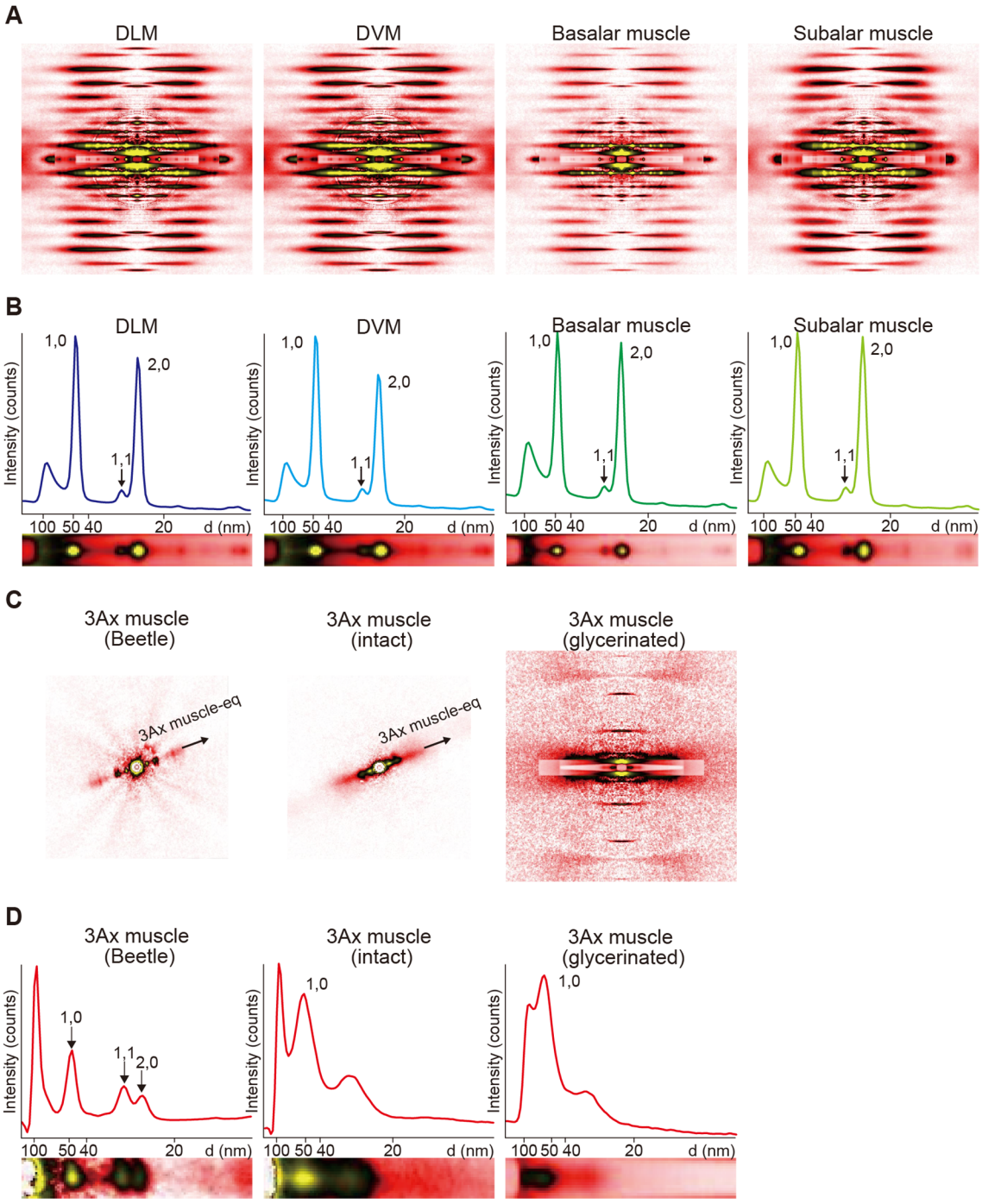

Figure S2 Synchrotron x-ray diffractions from flight muscles.

(*A* and *B*) Insect flight muscles in rigor condition. (*A*) The meridians of the patterns (the longitudinal axes of the muscle fibers) are oriented vertically. (*B*) Magnified views of a half of the equatorial reflections and their intensity profiles reproduced from (*A*). (*C* and *D*) The 3Ax muscle in the beetle (left), the 3Ax muscle dissected fresh from the beetle

(center, within half an hour from dissection) and the glycerinated fiber of the 3Ax muscle (right). (*C*) The orientation of the pattern is as recorded (left and center), or the meridian of the pattern from the glycerinated fiber (the longitudinal axes of the muscle fiber) is oriented vertically (right). (*D*) Magnified views of a half of the equatorial reflections and their intensity profiles reproduced from (*C*).

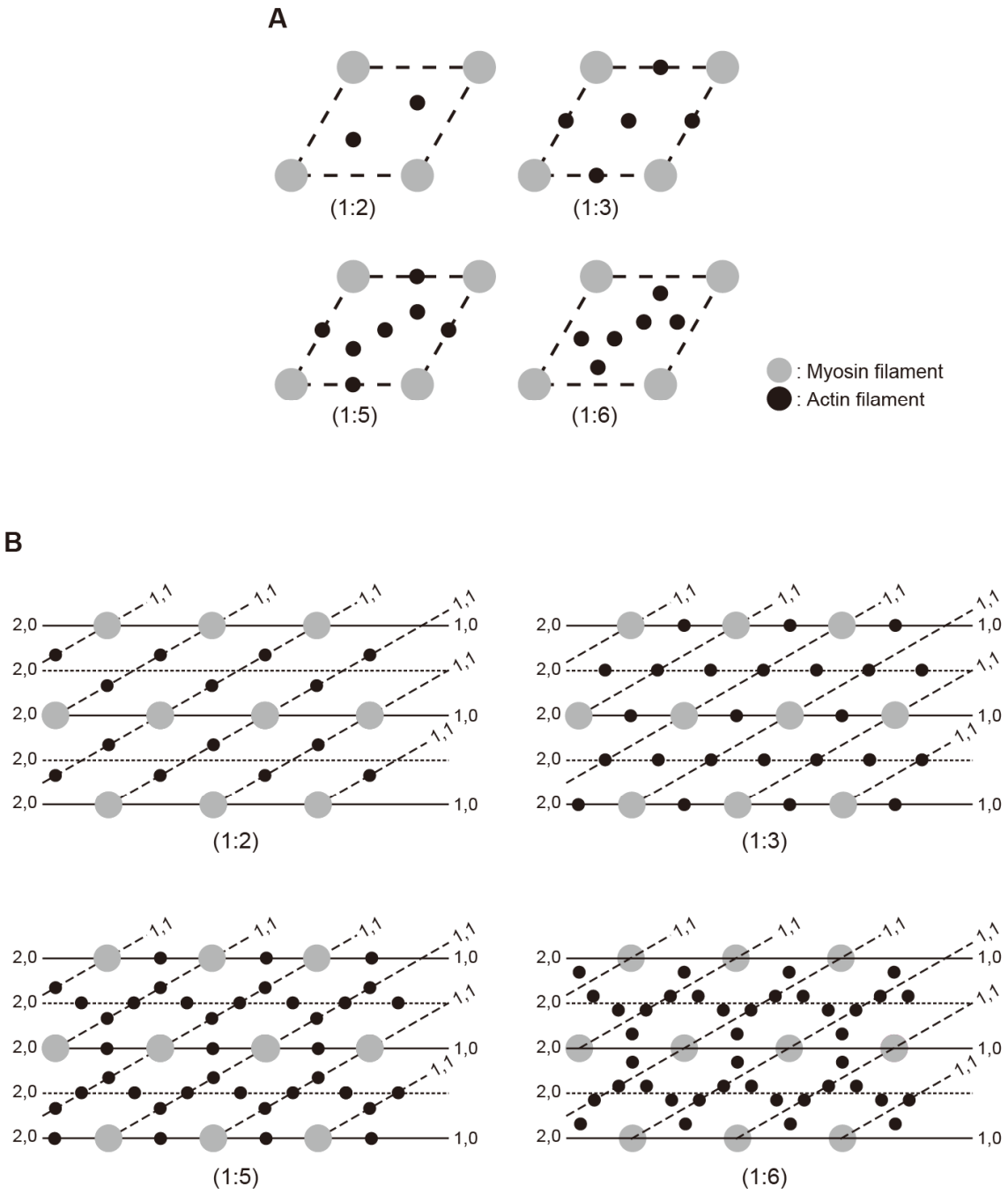

Figure S3 Schematic illustration of the various filament lattices.

(*A*) Representative arrangements of thick (myosin) and thin (actin) filaments. (*B*) The arrangement of thick and thin filaments in 1 : 2, 1 : 3, 1 : 5 and 1 : 6 lattices. The 1,0, 1,1 and 2,0 planes are shown by solid, broken and dotted lines, respectively. The thick-to-thin filament ratio can be inferred from the comparable intensities of 1,1 and 2,0 reflections in x-ray diffraction patterns. See Supplementary Discussion for details.

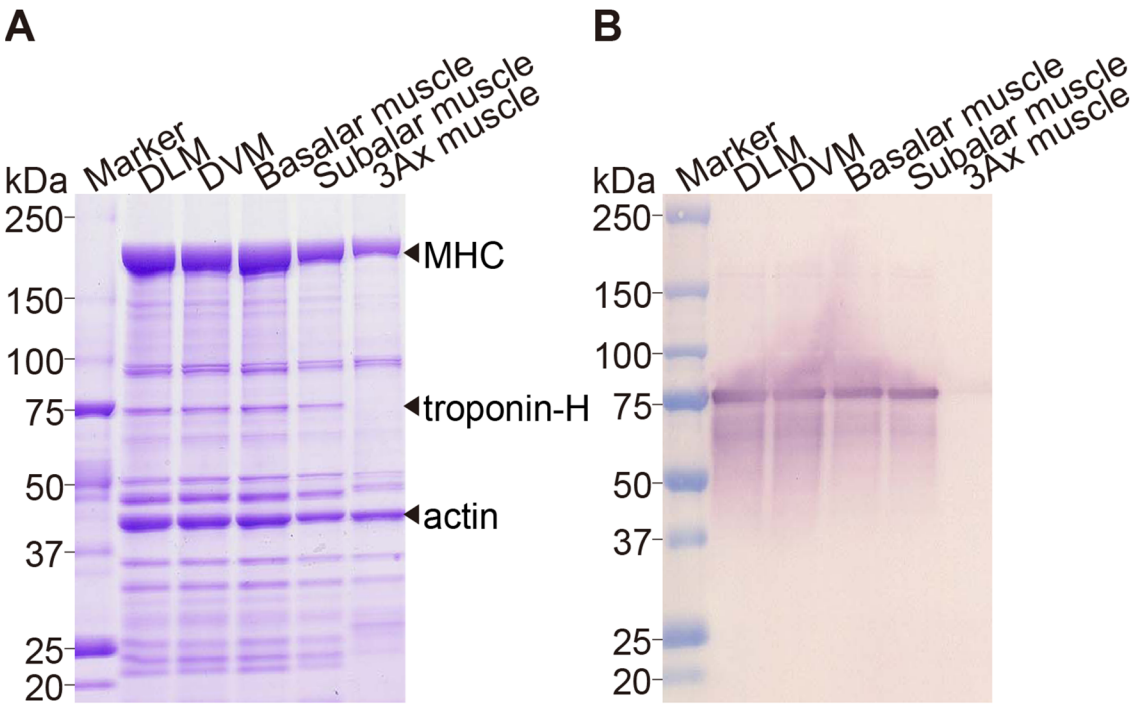

Figure S4 SDS-PAGE and immunoblotting of flight muscles

(*A*) SDS-PAGE of muscle fibers. Note that the bands corresponding to troponin-H are absent in the 3Ax muscle, and the lower mass regions show different expression patterns between the 3Ax muscle and other flight muscles. (*B*) Immunoblot analysis against troponin-H (MAC143).

Table S1 Sarcomere, myosin filament and actin filament lengths and A-band width determined by light microscopy.

Phase-contrast microscopy

Muscle	Sarcomere length (μm)	Myosin filament length (μm)
Dorsal longitudinal muscle (DLM)	3.40 ± 0.16 (n=31, N=3)	2.55 ± 0.08 (n=31, N=3)
Dorso-ventral muscle (DVM)	3.39 ± 0.11 (n=33, N=3)	2.50 ± 0.09 (n=33, N=3)
Basalar muscle	3.39 ± 0.14 (n=31, N=3)	2.48 ± 0.14 (n=33, N=3)
Subalar muscle	3.52 ± 0.12 (n=35, N=3)	2.70 ± 0.90 (n=32, N=3)
3Ax muscle	5.15 ± 0.26 (n=29, N=3)	3.27 ± 0.29 (n=30, N=3)
Leg muscle	6.34 ± 0.27 (n=28, N=3)	4.87 ± 0.19 (n=33, N=3)

n, the number of sarcomeres. N, the number of beetles. (mean ± SD)

Fluorescence microscopy

Muscle	Sarcomere length (μm)	Myosin filament length (μm)	Actin filament length (μm)
Dorsal longitudinal muscle (DLM)	3.29 ± 0.11 (n=301, N=5)	2.49 ± 0.14 (n=212, N=5)	1.42 ± 0.05 (n=292, N=5)
Dorso-ventral muscle (DVM)	3.21 ± 0.11 (n=273, N=5)	2.40 ± 0.15 (n=131, N=5)	1.38 ± 0.08 (n=204, N=5)
Basalar muscle	3.18 ± 0.09 (n=300, N=5)	2.33 ± 0.17 (n=128, N=5)	1.34 ± 0.07 (n=302, N=5)
Subalar muscle	3.50 ± 0.14 (n=301, N=5)	2.61 ± 0.25 (n=113, N=5)	1.54 ± 0.06 (n=152, N=5)
3Ax muscle	4.89 ± 0.33 (n=200, N=5)	3.27 ± 0.32 (n=139, N=5)	2.00 ± 0.15 (n=146, N=5)
Leg muscle	6.31 ± 0.42 (n=238, N=5)	5.12 ± 0.41 (n=136, N=5)	2.92 ± 0.32 (n=144, N=5)

n, the number of sarcomeres. N, the number of beetles. (mean ± SD)

Table S2 Summary of significance test results for optical microscopy analyses

S.L. by phase-contrast microscopy

	DLM	DVM	Basalar	Subalar	3Ax muscle	Leg
DLM		0.99939	0.99914	0.10298	9.22×10^{-8}	$< 1\times10^{-10}$
DVM	0.99939		1	0.03668	1.39×10^{-8}	$< 1\times10^{-10}$
Basalar	0.99914	1		0.03409	1.40×10^{-8}	$< 1\times10^{-10}$
Subalar	0.10298	0.03668	0.03409		7.69×10^{-7}	$< 1\times10^{-10}$
3Ax muscle	9.22×10^{-8}	1.39×10^{-8}	1.40×10^{-8}	7.69×10^{-7}		1.64×10^{-8}
Leg	$< 1\times10^{-10}$	$< 1\times10^{-10}$	$< 1\times10^{-10}$	$< 1\times10^{-10}$	1.64×10^{-8}	

A-band by phase-contrast microscopy

	DLM	DVM	Basalar	Subalar	3Ax muscle	Leg
DLM		0.76657	0.42506	0.00109	$< 1\times10^{-10}$	$< 1\times10^{-10}$
DVM	0.76657		0.99423	2.41×10^{-6}	$< 1\times10^{-10}$	$< 1\times10^{-10}$
Basalar	0.42506	0.99423		1.69×10^{-7}	1.33×10^{-8}	$< 1\times10^{-10}$
Subalar	0.00109	2.41×10^{-6}	1.69×10^{-7}		$< 1\times10^{-10}$	$< 1\times10^{-10}$
3Ax muscle	$< 1\times10^{-10}$	$< 1\times10^{-10}$	1.33×10^{-8}	$< 1\times10^{-10}$		$< 1\times10^{-10}$
Leg	$< 1\times10^{-10}$	$< 1\times10^{-10}$	$< 1\times10^{-10}$	$< 1\times10^{-10}$	$< 1\times10^{-10}$	

S.L. by fluorescence microscopy

	DLM	DVM	Basalar	Subalar	3Ax muscle	Leg
DLM		1.63×10^{-5}	3.89×10^{-9}	8.54×10^{-10}	$< 1\times10^{-10}$	$< 1\times10^{-10}$
DVM	1.63×10^{-5}		0.365	$< 1\times10^{-10}$	$< 1\times10^{-10}$	$< 1\times10^{-10}$
Basalar	3.89×10^{-9}	0.365		$< 1\times10^{-10}$	$< 1\times10^{-10}$	$< 1\times10^{-10}$
Subalar	8.54×10^{-10}	$< 1\times10^{-10}$	$< 1\times10^{-10}$		$< 1\times10^{-10}$	$< 1\times10^{-10}$
3Ax muscle	$< 1\times10^{-10}$	$< 1\times10^{-10}$	$< 1\times10^{-10}$	$< 1\times10^{-10}$		$< 1\times10^{-10}$
Leg	$< 1\times10^{-10}$	$< 1\times10^{-10}$	$< 1\times10^{-10}$	$< 1\times10^{-10}$	$< 1\times10^{-10}$	

Actin filament by fluorescence microscopy

	DLM	DVM	Basalar	Subalar	3Ax muscle	Leg
DLM		0.02735	$< 1\times10^{-10}$	$< 1\times10^{-10}$	$< 1\times10^{-10}$	$< 1\times10^{-10}$
DVM	0.02735		0.0315	$< 1\times10^{-10}$	$< 1\times10^{-10}$	$< 1\times10^{-10}$
Basalar	$< 1\times10^{-10}$	0.0315		$< 1\times10^{-10}$	$< 1\times10^{-10}$	$< 1\times10^{-10}$
Subalar	$< 1\times10^{-10}$	$< 1\times10^{-10}$	$< 1\times10^{-10}$		1.17×10^{-8}	$< 1\times10^{-10}$
3Ax muscle	$< 1\times10^{-10}$	$< 1\times10^{-10}$	$< 1\times10^{-10}$	1.17×10^{-8}		$< 1\times10^{-10}$
Leg	$< 1\times10^{-10}$	$< 1\times10^{-10}$	$< 1\times10^{-10}$	$< 1\times10^{-10}$	$< 1\times10^{-10}$	

Myosin filament by fluorescence microscopy

	DLM	DVM	Basalar	Subalar	3Ax muscle	Leg
DLM		0.04182	7.37×10^{-7}	2.77×10^{-4}	4.67×10^{-9}	$< 1\times10^{-10}$
DVM	0.04182		0.1772	$< 1\times10^{-10}$	4.58×10^{-9}	$< 1\times10^{-10}$
Basalar	7.37×10^{-7}	0.1772		$< 1\times10^{-10}$	5.28×10^{-9}	$< 1\times10^{-10}$
Subalar	2.77×10^{-4}	$< 1\times10^{-10}$	$< 1\times10^{-10}$		$< 1\times10^{-10}$	$< 1\times10^{-10}$
3Ax muscle	4.67×10^{-9}	4.58×10^{-9}	5.28×10^{-9}	$< 1\times10^{-10}$		$< 1\times10^{-10}$
Leg	$< 1\times10^{-10}$	$< 1\times10^{-10}$	$< 1\times10^{-10}$	$< 1\times10^{-10}$	$< 1\times10^{-10}$	

Data were statistically compared by using one-way ANOVA with Tukey-Kramer's test. Values of significance tests were described in Figure 2 as: NS, not significant; *, $p < 0.05$; **, $p < 0.01$; and ***, $p < 0.001$.

Table S3 The 1,0 lattice spacing (*d1,0*) and interfilament distance (the distance between the thick filaments) determined by x-ray diffraction study.

Muscle	*d1,0* (nm)	Interfilament distance (nm)
DLM	50.2 ± 0.2 (N=3, n=5)	58.0 ± 0.3 (N=3, n=5)
DVM	50.0 ± 0.4 (N=3, n=5)	57.7 ± 0.4 (N=3, n=5)
Basalar muscle	50.3 ± 0.3 (N=2, n=3)	58.1 ± 0.4 (N=2, n=3)
Subalar muscle	50.3 ± 0.3 (N=2, n=3)	58.1 ± 0.4 (N=2, n=3)
3Ax muscle	48.5 ± 1.2 (N=4, n=7)	56.0 ± 1.4 (N=4, n=7)
Leg muscle	50.1 ± 1.1 (N=2, n=2)	57.8 ± 1.2 (N=2, n=2)

n, the number of samples. N, the number of beetles.

The interfilament distance was determined by $d1,0 \times 2/\sqrt{3}$.

(mean ± SD)

Table S4 Summary of the length of muscle filaments and sarcomeres, the thick-to-thin filament ratio and the interfilament distance in previous studies from various species.

Muscle	Sarcomere length (μm)	Thick filament length (μm)	Thin filament length (μm)	Thick-to-thin filament ratio	Interfilament distance (nm)	References
Cockroach femur	6.4	4.5	2.3	5	57.0	(47,48)
Cockroach flight	NA	2.7	NA	3.8	NA	(47)
Cockroach intersegmental	7.8-8.3	3.6-4.1	4.1*	6	NA	(49)
Crab leg (long)	10.6*	5*	5*	6	59.4	(33,34)
Crab pink eye-raiser	4-12	NA	NA	7	50.0*	(35)
Crayfish leg	9.6	about 6	NA	6	62.1	(36,37)
Dog heart	1.90-1.98	1.5*	0.9*	2	NA	(38,39)
Dragonfly DVM	2.3	2.04*	1.08*	3*	NA	(40)
Frog sartorius	2.3	1.65	1*	2	42.1	(41)
Lethocerus femur	4.6*	3.1-3.8	1.8-2.2	4.8-5.2	NA	(16)
Lethocerus flight (indirect muscle)	2.6	2.3	1.2*	3	53.0	(43,44)
Lobster claw	12.4	6	4.5*	12	50.0	(18)
Lobster tail	4.0-5.2	3.4	1.7*	3	43.5	(18)
Rabbit psoas	1.8*	1.3*	0.8*	2	50.0	(16,29, 42)
Rhodnius prolixus ventral intersegmental abdominal muscles	8-10	6.6*	4.9*	6	NA	(45)
Scallop striated adductor	2.2-3.7	1.76	1.01	5-6	60.6	(46)
Tarantula femur	5	4.0-4.7	2.1*	about 5	NA	(17)

*, values were estimated based on the electron microscopy images provided.

Supporting Discussion

The calculated effect of lattice type on equatorial intensities

Different lattice types have different effects on the equatorial intensities. By assuming an ideal hexagonal lattice and that all the mass of the filament is only at the center of the filament, Elliott *et al.* (1) and Iwamoto (2) have calculated the intensities of equatorial reflections in 1 : 2 (vertebrate skeletal muscle type) and 1 : 3 (flight muscle type) lattices. Briefly, in 1 : 2 lattices, the phases of two thin filaments in a unit cell with respect to that of the thick filament are $2\pi/3$ and $4\pi/3$ for 1,0; 0 and 0 for 1,1; and $4\pi/3$ and $8\pi/3$ for 2,0 (Fig. S3). The amplitudes of equatorial intensities can be calculated by summing these structural factors; $F(1,0) = F(2,0) = \mathrm{FM} - \mathrm{FA}$, and $F(1,1) = \mathrm{FM} + 2\mathrm{FA}$, where FM and FA are the amplitudes of scattering factors for the thick (myosin) and thin (actin) filaments, respectively. The strong 1,1 and the weak 2,0 reflections are therefore expected. In 1 : 3 lattices, the amplitudes are $F(1,0) = F(1,1) = \mathrm{FM} - \mathrm{FA}$, and $F(2,0) = \mathrm{FM} + 3\mathrm{FA}$. In this lattice, the 1,1 reflection is expected to be substantially weaker than 2,0 (cf. Fig. 3 *B*)

The 1 : 5 lattice is the superposition of the 1 : 2 and 1 : 3 lattices (Fig. S3 *A*). Thus, under the same assumptions, the amplitudes in the 1 : 5 lattice can be calculated as the sum of the 1 : 2 and 1 : 3 lattices; i.e., $F(1,0) = \mathrm{FM} - 2\mathrm{FA}$, $F(1,1) = \mathrm{FM} + \mathrm{FA}$, and $F(2,0) = \mathrm{FM} + 2\mathrm{FA}$.

In the 1 : 6 lattice (Fig. S3 *A*), the phases of six thin filaments are $(2\pi\ (3 - \sqrt{3}))/3$, $(2\pi\ (2\sqrt{3} - 3))/3$, $(2\pi\ (3 - \sqrt{3}))/3$, $2\pi\sqrt{3}/3$, $2\pi\ (6 - 2\sqrt{3}))/3$ and $2\pi\sqrt{3}/3$ for 1,0; $2\pi\ (2 - \sqrt{3})$, $2\pi\ (\sqrt{3} - 1)$, 0, 0, $2\pi\ (2 - \sqrt{3})$ and $2\pi\ (\sqrt{3} - 1)$ for 1,1; and $(2\pi\ (6 - 2\sqrt{3}))/3$, $(2\pi\ (4\sqrt{3} - 6))/3$, $(2\pi\ (6 - 2\sqrt{3}))/3$, $4\pi\sqrt{3}/3$, $(2\pi\ (12 - 4\sqrt{3}))/3$ and $4\pi\sqrt{3}/3$ for 2,0. Thus, the amplitudes are calculated to be; $F(1,0) = \mathrm{FM} - 2.41\mathrm{FA}$, $F(1,1) = \mathrm{FM} + 1.55\mathrm{FA}$, and $F(2,0) = \mathrm{FM} + 1.53\mathrm{FA}$. Different from 1 : 2 and 1 : 3 lattices, the 1,1 and 2,0 reflections are estimated to be comparable in 1 : 5 and 1 : 6 lattices.

Supporting References

1. Elliott, G. F., J. Lowy, and C.R. Worthington. 1963. An X-ray and light-diffraction study of the filament lattice of striated muscle in the living state and in rigor. J. Mol. Biol. 6: 295–305.

2. Iwamoto, H. 2013. Flight muscle-specific Pro-Ala-rich extension of troponin is important for maintaining the insect-type myofilament lattice integrity. J. Struct. Biol. 183: 33–39.